Journal of Power Sources 195 (2010) 6740–6747

Contents lists available at ScienceDirect

Journal of Power Sources

journal homepage: www.elsevier.com/locate/jpowsour

Electrochemical catalytic activities of nanoporous palladium rods for methanol electro-oxidation

Xiaoguang Wang, Weimin Wang, Zhen Qi, Changchun Zhao, Hong Ji, Zhonghua Zhang*

Key Laboratory for Liquid-Solid Structural Evolution and Processing of Materials (MOE), School of Materials Science and Engineering, Shandong University, Jingshi Road 73, Jinan 250061, PR China

ARTICLE INFO

Article history:
Received 19 March 2010
Accepted 29 March 2010
Available online 3 April 2010

Keywords:
Nanoporous palladium rods
Dealloying
Electrocatalysis
Fuel cells

ABSTRACT

A novel electrocatalyst, nanoporous palladium (npPd) rods can be facilely fabricated by dealloying a binary $Al_{80}Pd_{20}$ alloy in a 5 wt.% HCl aqueous solution under free corrosion conditions. The microstructure of these nanoporous palladium rods has been characterized using scanning electron microscopy and transmission electron microscopy. The results show that each Pd rod is several microns in length and several hundred nanometers in diameter. Moreover, all the rods exhibit a typical three-dimensional bicontinuous interpenetrating ligament-channel structure with length scale of 15–20 nm. The electrochemical experiments demonstrate that these peculiar nanoporous palladium rods (mixed with Vulcan XC-72 carbon powders to form a npPd/C catalyst) reveal a superior electrocatalytic performance toward methanol oxidation in the alkaline media. In addition, the electrocatalytic activity obviously depends on the metal loading on the electrode and will reach to the highest level (223.52 mA mg^{-1}) when applying 0.4 mg cm^{-2} metal loading on the electrode. Moreover, a competing adsorption mechanism should exist when performing methanol oxidation on the surface of npPd rods, and the electro-oxidation reaction is a diffusion-controlled electrochemical process. Due to the advantages of simplicity and high efficiency in the mass production, the npPd rods can act as a promising candidate for the anode catalyst for direct methanol fuel cells (DMFCs).

1. Introduction

The electrochemical oxidation of small organic molecules (SOMs) has been widely studied due to their potential utilization as fuel in energy conversion systems. The main reason is related to their rich abundance, facility of storage/handling, and primarily their energy density. Moreover, due to their simple molecular structures they should exhibit an excellent electrochemical activity and reveal a high energy conversion efficiency in the fuel cells [1–3].

The electrochemical oxidation of fuels requires the use of a catalyst to achieve the high current densities for practical applications. Thus the high surface area and intrinsic electrochemical feature are key factors for the promising electrocatalytic materials. Nowadays, porous metallic materials, especially nanoporous gold, platinum, and nickel, have received increasing attention in view of their potential applications in catalysts, chemical sensors, selective filtration, fuel cells and microfluidic flow controllers, etc. [4–7]. Nanoporous metals can be prepared by selectively etching a single phase or multiple phase alloy that consists of two kinds of metals with different chemical activities under appropriate corrosion conditions. This process is called dealloying and the most famous nanoporous metal fabricated by dealloying is the nanoporous gold (NPG), which can be fabricated by selective dissolution of Ag out of Ag-Au alloys with a single phase solid solubility across all compositions [4]. In addition, the dealloying phenomenon can also be observed in several other systems and used to fabricate corresponding porous metals. These alloy systems can include single phase solutions (e.g. Ni–Cu [7], Mn–Cu [8], Pt–Cu [9]), intermetallic compounds (e.g. Cu_3Au [10], Al_2Au [11]), two-phase alloys (e.g. Al–Ag [12], Cu–Zr [13], Al–Cu [14], Mg–Cu [15]), and even amorphous metallic glasses (e.g. Pt–Si [6], Pd–Ni–P [16]). Following the dissolution of the active component in a dealloying process, the relevant inert metal atoms can be retained and undergo a complex diffusion and agglomeration evolution to form a continuous nanosized porous structure. From a practical catalysis viewpoint, these nanoporous metals (Au, Pt, Ag, Cu, etc.) with large specific surface areas can greatly improve the utilization of surface active sites and will have a promising prospect in the catalysis field.

At the present time, as an alternative to the more expensive Pt, Pd has been used as the catalyst for various applications. Significantly, Pd nanostructures with larger specific surface areas and more active centers have been extensively investigated in various electrochemical reactions to explore their potential industrial

* Corresponding author. Tel.: +86 531 88396978; fax: +86 531 88395011.
E-mail address: zh_zhang@sdu.edu.cn (Z. Zhang).

0378-7753/$ – see front matter © 2010 Elsevier B.V. All rights reserved.
doi:10.1016/j.jpowsour.2010.03.098

applications. To date, Pd nanoparticles [17], Pd nanoplate arrays [18], Pd nanotrees [19], Pd nanowires [20], Pd nanoflowers [21] and so forth, have been synthesized through chemical reduction reactions by several groups and these microstructures reveal well electrocatalytic activities toward methanol and ethanol oxidation. However, little attention has been paid to nanoporous Pd (npPd) with a typical three-dimensional, bicontinuous, interpenetrating nanosized ligament-channel structure. In comparison with other nanostructures, the typical npPd structures are expected to have superior performances due to their inherent special morphology and characteristic, such as the open porosity, high surface area, as well as high structural stability with no agglomeration. Yu et al. [16] have synthesized npPd through electrochemical dealloying a ternary $Pd_{30}Ni_{50}P_{20}$ metallic glass, and have found that the as-prepared npPd exhibited well catalytic activity towards formic acid oxidation. Xu et al. [22] have also synthesized a nanotubular mesoporous bimetallic Pd/Cu catalyst based on a combination of dealloying and galvanic-replacement reaction. However, there still exist lots of drawbacks, such as the strict apparatus demanding, the greater dealloying driving force needed and time-consuming during dealloying, especially the complexity of the operation. Hence, it is urgent to develop a simple and efficient productive strategy so as to meet the requirement of industrial applications.

Recently, we have developed a facile route to synthesize nanoporous metals through dealloying of Al-based alloys, and have found that peculiar nanoporous Pd rod structures can be directly fabricated by dealloying of Al–Pd alloys in the 5 wt.% HCl aqueous solution [11]. At present, we are particularly interested in the electrocatalytic properties of the npPd rods for electro-oxidation of SOMs with an eye to their potential applications as high efficiency catalysts in SOMFCs. In this work, we aim to systematically study the influence of the loadings on the catalytic activities of the npPd rods towards methanol electro-oxidation in alkaline media, and further investigate the effects of the methanol concentration and potential scan rate on the catalytic activities at a given loading. To our best knowledge, this is the first work to systematically investigate the electrocatalytic properties of these novel npPd rods towards methanol electro-oxidation. Anyway, considering the advantages such as the easy access to raw materials, the simplicity and high efficiency in the synthesis process as well as the revealing enhanced electrocatalytic activity, this novel npPd rods structure is expected to act as a promising electrocatalyst in the direct methanol fuel cells (DMFCs).

2. Experimental

The $Al_{80}Pd_{20}$ (nominal composition, at.%) alloy ribbons were prepared by a melt spinning technique. The dealloying of the starting ribbons was performed at $90 \pm 5\,^{\circ}C$ in a 5 wt.% HCl solution until no visible bubbles emerged. The detailed synthesis procedure of npPd rods can be found elsewhere [11]. Microstructural characterization of the npPd rods was made using a scanning electron microscopy (LEO 1530 VP) and a transmission electron microscope (Philips CM 20). In addition, chemical composition of the as-dealloyed sample was determined using an energy dispersive X-ray analyzer which was attached to SEM. TEM specimens were prepared using a Gatan ion mill at 5 kV.

All electrochemical measurements were performed in a standard three-electrode cell using a LK 2005A Potentiostat. The corresponding npPd rods electrodes were prepared as follows: a certain mass of fine ground npPd rods samples (that is 2, 4, 6, 8, 10, 12 mg in the present work), 4 mg Vulcan XC-72 carbon powders, 300 μL isopropanol, and 100 μL Nafion solution (0.5 wt.%) were ultrasonically mixed. Then, 5 μL of the homogeneously mixed ink was placed on a freshly polished glassy carbon (GC) electrode with a diameter of 4 mm. Table 1 shows the loadings of the npPd rods on the GC electrodes. For clarity, the mass of the npPd rods on each GC electrode can be normalized to mass per cm^2. These electrodes were used as the working electrodes. The counter electrode was a bright Pt plate, and a saturated calomel electrode (SCE) or a Hg/HgO (1.0 M KOH) electrode (MMO) was used as the reference electrode, depending on the experimental requirements. Voltammetric behavior was characterized in a 0.5 M H_2SO_4 solution deaerated with N_2. The CO stripping experiments were performed by firstly maintaining the work electrode in the 0.5 M H_2SO_4 solution saturated with high purity CO gas at the potential of −0.09 V (vs. SCE) for the period of 600 s, and then transferring the electrode into a clean 0.5 M H_2SO_4 solution followed by linear potential scan at a scan rate of 50 mV s^{-1}. The electrocatalytic activity measurements were carried out in methanol and KOH mixed solutions. All electrochemical experiments were performed at ambient temperature (∼25 °C).

Table 1
Metal/carbon ratio and normalized loadings of the npPd rods on the GC electrodes.

	Metal content (mg)					
	2	4	6	8	10	12
Metal/carbon ratio	1/2	1/1	3/2	2/1	5/2	3/1
Normalized loadings (mg cm^{-2})	0.2	0.4	0.6	0.8	1.0	1.2

3. Results and discussion

Fig. 1(a) shows the section-view microstructure of the as-dealloyed npPd ribbons which are composed of hundreds of npPd rods. It is clear that the npPd rods exhibit several microns in length and hundreds of nanometers in diameter. Furthermore, these rods are surprisingly parallel with each other in a certain range forming clusters. For clarity, several parallel clusters are highlighted by the dot-dash lines in Fig. 1(a). The SEM image at a higher magnification (Fig. 1(b)) further verifies the peculiar parallel-oriented characteristic of the npPd rods in the neighboring region. In addition, the nanoporous structure can be clearly observed on the surface of the npPd rods. The fractured cross-section morphology of the npPd rods, highlighted by arrows in Fig. 1(c), also exhibits an open, bicontinuous interpenetrating ligament-channel structure, suggesting that the porous structure is three-dimensional in each npPd rod. As shown in Fig. 1(d), the TEM image further reveals the bicontinuous ligament-channel structure in the interior of the npPd rod, and the length scale of the ligaments/channels is in the scope of 15–20 nm. Moreover, the EDX analysis shows that almost all of Al was removed during dealloying in the hydrochloric acid circumstance and the residual Al is less than 1 at.% in the npPd ribbons. In addition, the selected-area electron diffraction and HRTEM observation demonstrate that the connecting ligaments in the npPd rods are composed of randomly oriented f.c.c. Pd nanocrystals with several nanometers in size [11]. The formation of these peculiar ligament-channel npPd rods may be ascribed to a typical two-phase dealloying process. In the initial preparation of the Al–Pd starting alloy, the primary Al_3Pd phase firstly precipitates from the $Al_{80}Pd_{20}$ melt in the form of clusters comprising parallel rods. Then the remaining melt transforms into the α-Al phase which exists in the interspace of the Al_3Pd rods. In the following dealloying process, the active α-Al phase was firstly leached away providing a large number of routeways through which the electrolyte can penetrate into the interior of the starting alloy ribbons [13]. Whereafter, the exposed parallel Al_3Pd crystals were continuously dealloyed giving rise to the formation of the nanoporous structure. To a certain extent, the parallel pattern of the columnar Al_3Pd crystals can be preserved into the resultant npPd rods during dealloying.

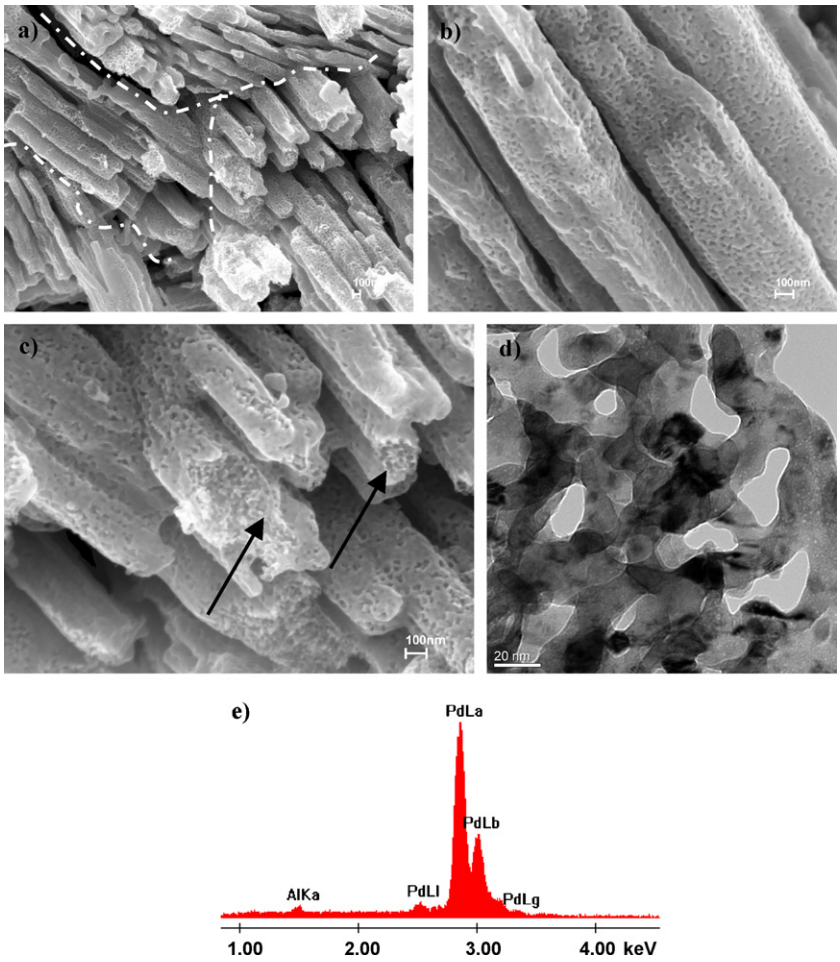

Fig. 1. (a–c) SEM and (d) TEM images showing the microstructure of the npPd rods through chemical dealloying of the $Al_{80}Pd_{20}$ alloy in the 5 wt.% HCl solution. (e) EDX spectrum showing the composition of the npPd rods.

The cyclic voltammograms (CVs) of all npPd rods electrodes are basically similar in the profile (not shown here). Fig. 2 shows a typical CV curve of the npPd rods electrode with 0.2 mg cm^{-2} metal loading in the 0.5 M H_2SO_4 solution. From the CVs, there exist two pairs of distinct current peaks in the hydrogen region (A and A′, B and B′), a broad oxidation current peak (C) and a characteristic reduction current peak (C′). The large pair of anodic peak (A and A′) at a more negative potential is related to H-desorption and -adsorption from the bulk together with the surface of ligaments in the npPd matrix while the small anodic peaks (B and B′) at a more positive potential ascribe to H-desorption and -adsorption on the surface of the npPd ligaments [23,24]. The broad oxidation peak C is ascribed to the formation of Pd surface oxide (PdO) and the corresponding peak C′ is caused by subsequent reduction of the oxide [25,26]. However, the processes of hydrogen adsorption, desorption, and evolution for the bulk Pd electrode are usually not separated from each other, which can be exemplified by a broad anodic peak in the CVs performed in the H_2SO_4 solution [27]. Grdeń et al. [23] have proposed that the changes in the amount of hydrogen manifested by the peak B are proportional to the changes of the real surface area of the Pd electrode. Meanwhile, it can be confirmed that a large number of Pd atoms are on the ligament surface owing to the open, bicontinuous interpenetrating ligament-channel structure of the npPd rods. Therefore, it is easy to observe peak B and B′ in the CV curve of the npPd electrode. The similar CV profiles are also observed for varieties of Pd nanostructured materials with large specific surface areas, such as Pd nanoparticles [28], ultrathin Pd film [27], and so on. Bartlett et al. [29] have argued that the electrochemical properties of nanostructured Pd differ significantly from those of the bulk Pd because the latter is able to absorb large quantities of hydrogen forming Pd hydride phases. Obviously, this kind of npPd rods can provide a possibility to separately study the individual processes involved in the hydrogen region.

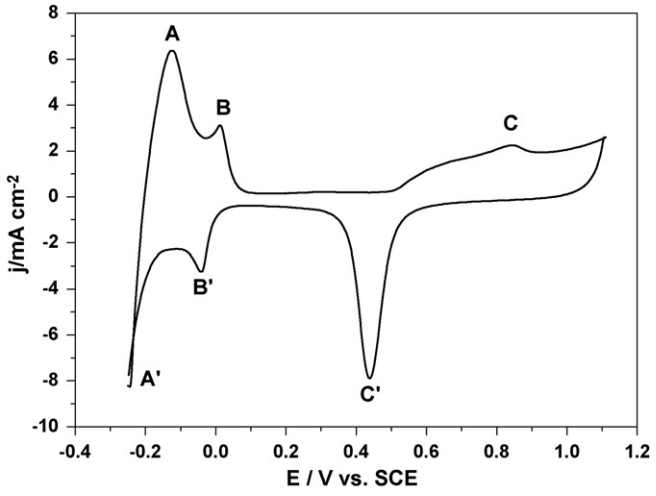

Fig. 2. CV curve for the npPd rods electrode in the 0.5 M H_2SO_4 solution deaerated with N_2. The scan rate of potential was 50 mV s^{-1}.

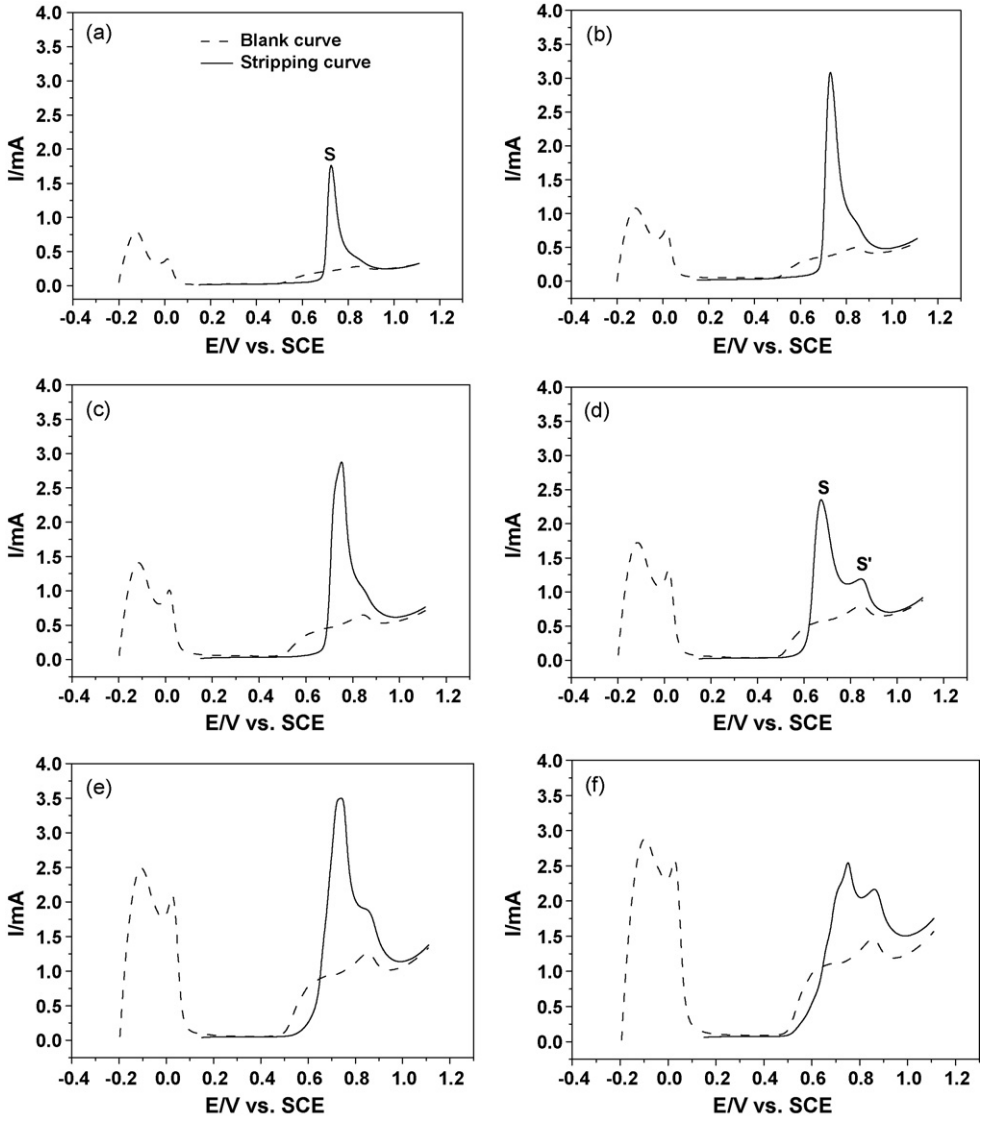

Fig. 3. CO stripping curves of the npPd rods electrodes with different metal loadings in the 0.5 M H_2SO_4 solution. The metal loading on the GC electrode was (a) 0.2 mg cm^{-2}, (b) 0.4 mg cm^{-2}, (c) 0.6 mg cm^{-2}, (d) 0.8 mg cm^{-2}, (e) 1.0 mg cm^{-2}, and (f) 1.2 mg cm^{-2}, respectively. The scan rate of potential was 50 mV s^{-1}.

Fig. 3 shows the CO stripping curves of the npPd rods electrodes with different Pd loadings in the 0.5 M H_2SO_4 solution. For the blank curve (dash line), two anodic peaks related to the hydrogen desorption/adsorption occur in the hydrogen region, which have been revealed detailedly in Fig. 2. Additionally, it is clear that the currents of both the anodic hydrogen desorption/adsorption peaks increase with increasing metal loadings from 0.2 to 1.2 mg cm^{-2} on the GC electrodes. For the stripping curve (solid line), an obvious anodic peak can be observed in the potential range from 0.5 to 1.0 V when performing linear sweeping voltammogram, which is associated with the oxidation of the pre-adsorbed CO. Meanwhile, a gradual transition from a single, well-defined CO stripping peak (marked by S) to a broader one can be observed. Moreover, an accompanying shoulder-like peak located at the positive side (marked by S′, Fig. 3(d)–(f)) becomes more and more obvious. It is well known that the stripping peak profile is sensitive to the composition and microstructure of metal particles [30], and several studies have found that the CO stripping curves associated with the Au–Pt [31,32], Pd–Ag [33], Pd–Ir [34], and Pt–Ru–P [35], will exhibit a contour change by variating the amount of the additive elements. Thus, the appearing shoulder peak may be caused by the existing residual Al in the Pd rods (Fig. 1(e)). With increasing metal loadings from 0.2 to 1.2 mg cm^{-2} on the GC electrodes, the current increase of the hydrogen desorption/adsorption peaks in the hydrogen region reveals the increase in the real electrochemical surface area, as proposed by Grdeń et al. [23]. However, it should be noted that Pd is intrinsically a hydrogen-storage metal and will inevitably absorb a certain amount of hydrogen, which is differ from that of the other metal Pt. In the case of Pt, the hydrogen region is always used to evaluate the electrochemical active surface area (EASA) by virtue of the hydrogen desorption/adsorption exclusively progressing on the surface [36,37]. However, for Pd, the hydrogen desorption/adsorption process originates not only from the ligament surface but from the interior of the ligaments of the npPd rods [38,39]. Thus, the enlargement of the hydrogen region cannot accurately indicate the increase in the real surface area, but should relate to a probable expression of the total amount of Pd on the electrode. In comparison, due to the fact that the CO monolayer is prone to adsorb on the surface active sites of Pd materials under a certain electrochemical circumstance, the CO stripping method has been widely used as an effective route to evaluate the EASA of Pd or Pd-based electrocatalysts [34,40]. Assuming the coulombic charge to surface area value of 420 μC cm^{-2} used for CO stripping on the surface of nanostructured Pd catalysts, the EASA and mass

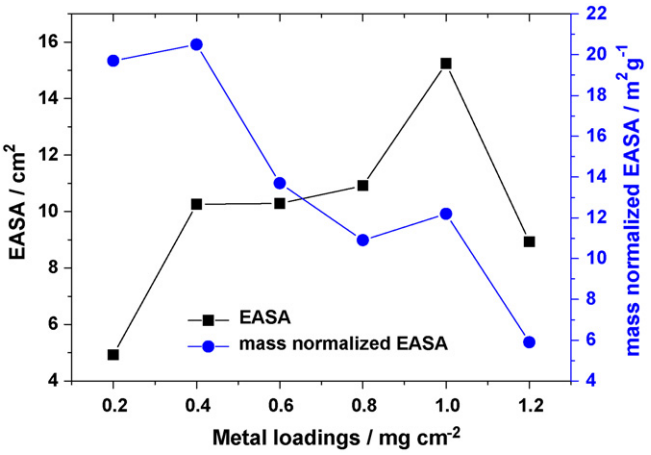

Fig. 4. Dependence of the electrochemical active surface area and the mass normalized electrochemical active surface area on the npPd rods loadings on the GC electrode.

normalized EASA can be calculated according to the integral of the corresponding CO stripping peak (from Fig. 3). The dependence of EASA and corresponding mass normalized EASA on the npPd loading is illustrated in Fig. 4. It can be seen that the EASA of the npPd rods increases nonlinearly with increasing npPd loadings from 0.2 to 1.0 mg cm^{-2} on the GC electrodes, and decreases sharply when the loading exceeds 1.0 mg cm^{-2}. However, the mass normalized EASA of the npPd rods gets to the highest level (20.5 m^2 g^{-1}) when the npPd loading attains to 0.4 mg cm^{-2}. The results also show that for the blending ratio of 4 mg npPd with 4 mg carbon powders there seems to be a proper quantity and proportion of the npPd rods in the npPd/C catalyst. With increasing the amount of npPd rods in the npPd/C mixture (a fixed amount of carbon powders, 4 mg), the accumulation of the Pd rods may occur and the uniformity of the npPd/C mixture will deteriorate. Hence, part of the npPd rods cannot be utilized adequately so as to result in the reduction of the EASA per mass of npPd rod electrode.

Fig. 5 shows the CV curves of the npPd rods electrodes with different metal loadings in the 0.5 M methanol + 1 M KOH solution. For clarity, the forward and backward scans of the methanol oxidation voltammograms are given in Fig. 5(a) and (b), respectively. Moreover, the detailed voltammetry parameters are illustrated in Table 2. It was observed that the onset potentials of methanol electrocatalytic oxidation on the npPd rods electrodes gradually shift to the more positive values with increasing Pd loading, however, the shift is very tiny and cannot be discerned from the forward scan curves. In addition, the current density for the methanol oxidation (mass catalytic activity) increases with the increasing amount of npPd rods loading and reaches up to the highest value (223.52 mA mg^{-1}) when the metal loading of the npPd rods being

Table 2
Cyclic voltammetry parameters for the methanol oxidation on the npPd rods electrodes with different metal loadings.

npPd rods loading (mg cm^{-2})	E_{op} (mV)	Forward scan		Backward scan	
		j_p (mA mg^{-1})	E_p (mV)	j_p (mA mg^{-1})	E_p (mV)
0.2	−404	166.94	−80	89.49	−143
0.4	−401	223.52	−42	146.18	−123
0.6	−400	208.20	−22	129.30	−117
0.8	−392	129.22	−28	104.74	−109
1.0	−390	118.61	−17	113.47	−89
1.2	−367	99.68	−22	90.01	−89

E_{op}: the onset potential; j_p: the oxidation peak current density; E_p: the oxidation peak potential.

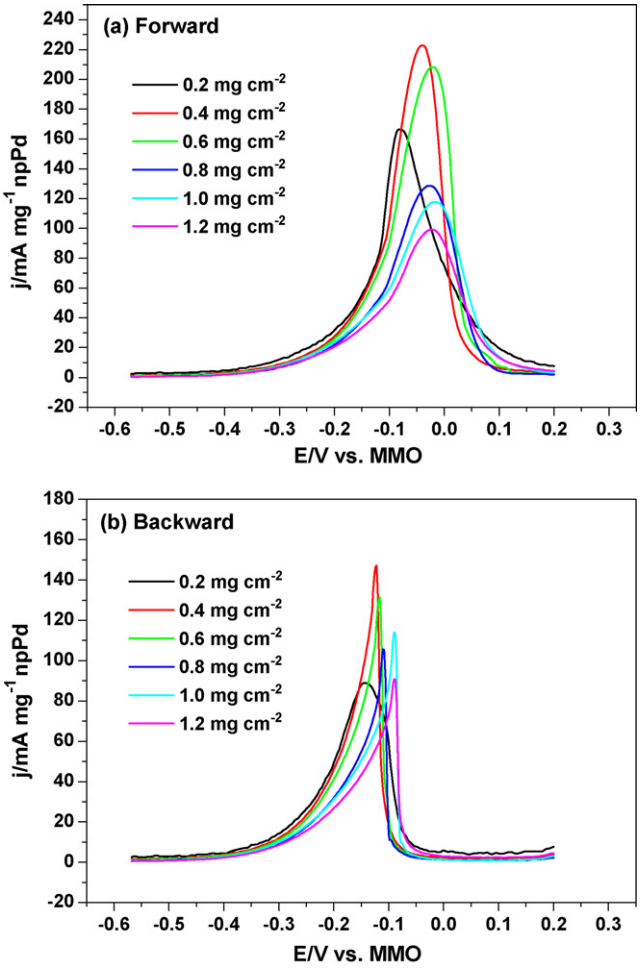

Fig. 5. CV curves of the npPd rods electrodes with different metal loadings in the 0.5 M methanol + 1 M KOH solution: (a) the forward scan and (b) the backward scan. The scan rate of potential was 10 mV s^{-1}.

0.4 mg cm^{-2} on the GC electrode. This mass activity is almost 5.6 times that of the Pd nanoflowers (~40 mA mg^{-1}) at the same scan rate [21]. When the npPd rod loading exceeds 0.4 mg cm^{-2}, the peak current decreases gradually, implying that the catalytic activity of the modified electrode decreases. The highest mass catalytic activity should be attributed to the highest EASA per mass of the npPd rods catalyst as well as the superior electrical contact and mass transfer process originating from the most suitable dispersion and volume ratio of metals in the npPd/C catalyst. In the previous research, it has been noted that there exists a dependence of the catalytic activity of alcohol electro-oxidation on the metal loading, especially for the metal Pt. Razmi et al. [41] have explored the effect of different Pt loadings at the carbon ceramic electrode surface on the oxidation of methanol and ethanol, and have found that the anodic peak current of methanol and ethanol oxidation increases with the increasing of the platinum loading from 0.2 to 2 mg cm^{-2} and then remains constant for the optimum Pt amount of 2–3 mg cm^{-2}. However, the anodic peak current decreases with continuously increasing the Pt loading to 4 mg cm^{-2}. Zhou et al. [42] have fabricated a novel platinum–poly(5-nitroindole) (Pt/PNI) composite catalyst and also investigated the effect of Pt loading on methanol oxidation on Pt/PNI/GC electrode at a fixed mass of PNI film. They have found that the peak current density increases with the increasing of Pt loading, reaches a maximum value at the Pt loading of 0.12 mg cm^{-2}, and then the peak current decreases when the Pt loading exceeds 0.12 mg cm^{-2}. Obviously, there exists

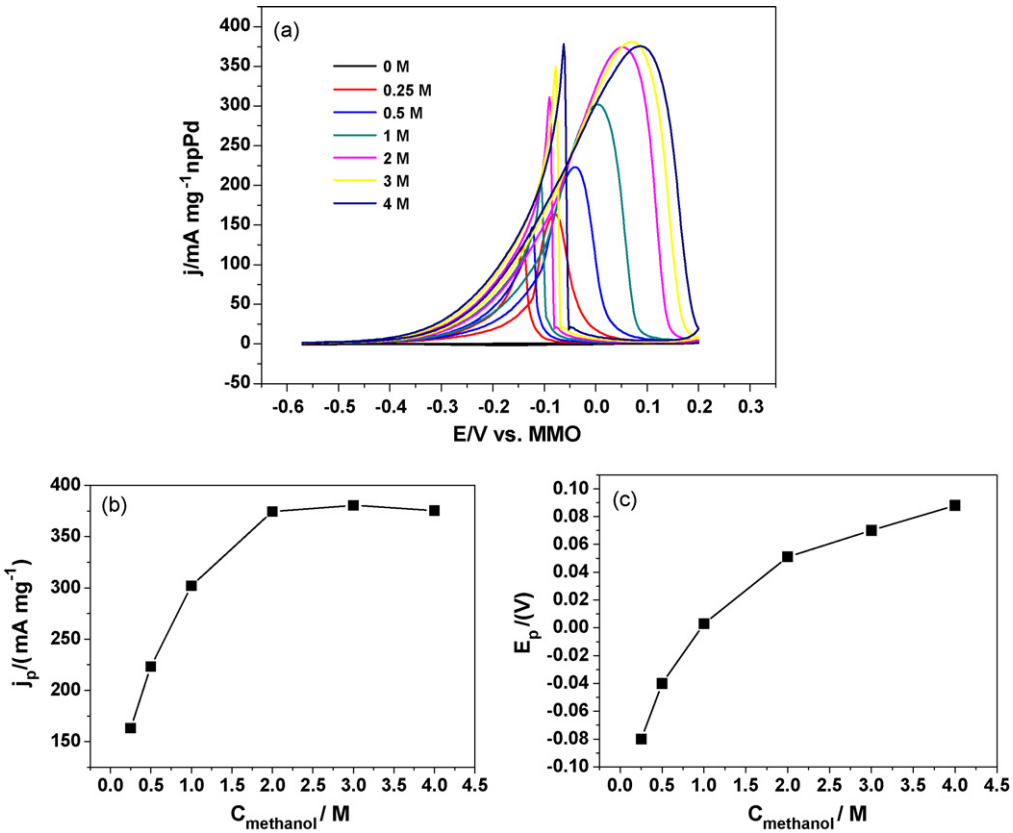

Fig. 6. (a) CV curves of the methanol electro-oxidation on the npPd rods electrode (with the 0.4 mg cm^{-2} npPd loading) in the 1.0 M KOH solutions containing methanol of various concentrations. (b) Plots of forward anodic peak current and (c) peak potential as a function of the methanol concentrations. The scan rate of potential was 10 mV s^{-1}.

a critical amount of metal loading corresponding to the maximum catalytic activity for the npPd rod catalyst mentioned here. On the one hand, metal particles are almost uniformly deposited on the surface of electrode at the lower metal loadings, which can cause an enhancement in the electrocatalytic activity of the modified electrode. When the metal loading is further increased, the metal particles agglomerate and reduce the amount of three-phase reaction interface so that the electrochemical active area and catalytic activity per mass correspondingly decrease. On the other hand, the discrepancy of the critical value related to the different metals may result from the dissimilar morphology of the metal particles, different reaction circumstance as well as the distinct nature of the catalyst support materials, such as the different metal dispersivity or electronic interaction. It is well known that the oxidation current peak located in the forward scan is correlated with the oxidation of freshly chemisorbed methanol molecules [43–45], and is usually used to evaluate the catalytic activity of electrocatalyst, as discussed above. However, there still exists much controversy with regard to the origin of the oxidation peak in the backward scan. Some researchers deemed that the reverse anodic current peak originated from the removal of the incompletely oxidized carbonaceous species adsorbed on the surface of the electrode rather than caused by freshly chemisorbed species [43–52]. These poisonous intermediate species (i.e. CO, $HCOO^-$ and HCO^-) may derive from those partially dehydrogenated methanol molecules in the forward potential scan and are mostly in the form of linearly bonded M=C=O (M: Pt or Pd) [21,53–57]. Besides, the ratio of the forward anodic peak current (I_f) to the reverse anodic peak current (I_b) was considered to describe the catalyst tolerance to accumulation of carbonaceous species in some degree [22,58–64]. At present, however, other researchers believed that the reverse current peak cannot ascribe to the intermediate species removal but rather still relate to the oxidation of the methanol molecules in the electrolyte [65–67]. In addition, Yajima et al. [68,69] have studied the electro-oxidation of methanol on the Pt by virtue of in situ ATR-FTIR spectroscopy, and have found that the adsorbed CO, which is dehydrogenated species from methanol, is oxidized at the potential more positive than 0.6 V (RHE). So it is reasonable to assume that there is no adsorbed CO species on the electrode when the potential reaches the anodic limit. Additionally, as the positive-going sweep proceeds, more Pd oxide covers the reactive surface of the npPd rods. The formation of the oxide layer can block the adsorption of the reactive species onto the Pd surface and thus bring about the decrease of the methanol oxidation current [65–67]. In the reverse potential scan, the Pd active sites are recovered by electroreduction of the Pd oxide, so that the freshly chemisorbed methanol can be re-oxidized in the methanol oxidation potential range. Obviously, the higher the potential is, the higher oxide coverage will attain. Since the oxidation/reduction of the Pd is an irreversible reaction, the higher oxide coverage, the lower potential is required for the reduction. Therefore, the current peak on the backward scan depends on the upper potential limit of the forward scan. According to the Pd electrochemical characteristic, the applied upper potential limit is located in the region of surface Pd oxide formation [48,67]. It can be concluded that the latter viewpoint is more reasonable. Besides, in the forward potential scan, some dehydrogenated intermediates ($HCOO^-$ and HCO^-) may desorb from the electrode surface and diffuse into the electrolyte, prior to being complete oxidation. The re-adsorption and oxidation of these species should also contribute to the increase of the reverse oxidation current. Of course, further research is still urgent and required.

Fig. 6(a) shows the CV curves of electrocatalytic oxidation towards methanol with different concentrations in the 1.0 M KOH

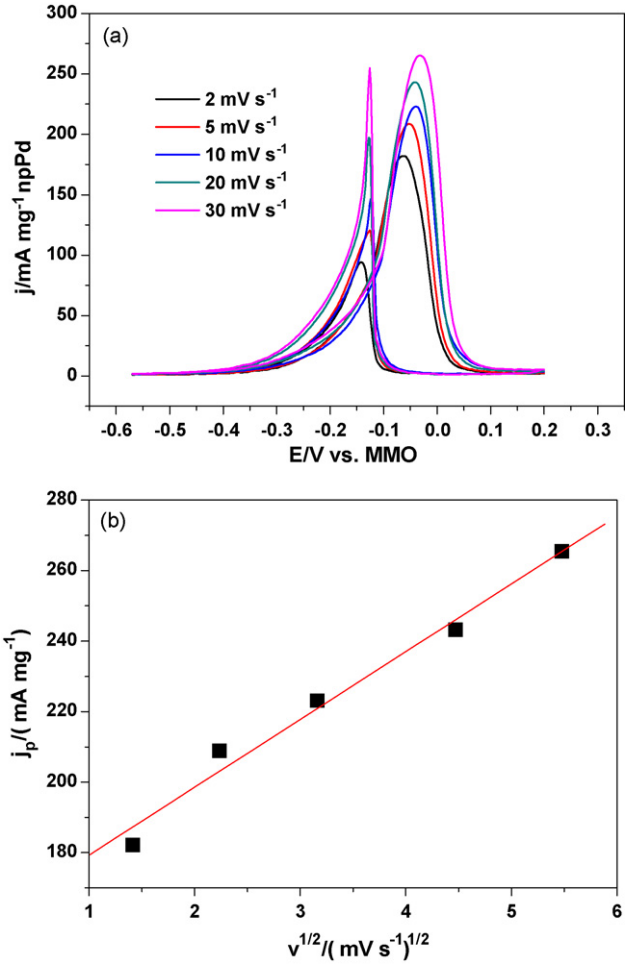

Fig. 7. (a) CV curves of the methanol electro-oxidation on the npPd rods electrode (with the 0.4 mg cm^{-2} loading) at different scan rates in the 0.5 M methanol + 1.0 M KOH solution, and (b) plot of forward anodic peak current density vs. the square root of the scan rate of potential.

solution on the npPd rods electrode (with the 0.4 mg cm^{-2} metal loading). In the methanol-free KOH solution, there are no electrocatalytic oxidation current signals and the CV curve only reveals the oxidation and reduction of the surface Pd atoms in alkaline solutions. Hence, the CV curve exhibits a tiny profile as compared to that performed in the methanol-contained solutions. In addition, it is noticeable that the oxidation peak current density firstly increases as the methanol concentration increases up to 2 M, and then trends to level-off with further increasing methanol concentration to 4 M (Fig. 6(b)). Moreover, the oxidation current peak shifts to the more positive potential with increasing methanol concentration in the KOH solution as shown in Fig. 6(c). It should be noted that the positive shift extent of the oxidation peak potential gradually becomes less when the methanol concentration increases from 0.25 to 4 M in the KOH solution. In the process of ethanol oxidation on the polycrystalline Pd electrode in alkaline media, there exists a complex process involving ethoxyl ($(CH_3CO)_{ads}$) and hydroxyl (OH_{ads}) competing adsorption on the surface of the Pd electrode [67]. Therefore, it is reasonable to assume that there exists an analogous competing adsorption of methoxyl ($(CH_3O)_{ads}$) and hydroxyl (OH_{ads}) on the surface of the Pd electrode during the methanol oxidation process in the alkaline circumstance [70–72]. On the one hand, the adsorption of $(CH_3O)_{ads}$ on the surface of the ligaments in the npPd rods can be accelerated with the increasing of methanol concentration, giving rise to the increase in the peak current of the methanol oxidation reaction. On the other hand, the Pd–OH_{ads} coverage can be gradually changed with the increasing of the methanol concentration. As to the lower methanol concentration of less than 2 M in the KOH solutions, the adsorption of $(CH_3O)_{ads}$ is far from saturation and rarely blocks the adsorption of OH_{ads}. As the coverage of the adsorbate ($(CH_3O)_{ads}$) increases to a certain value (when the methanol concentration exceeds 2 M), the adsorption of $(CH_3O)_{ads}$ on the ligament surface will be dominant, and the adsorption of the OH_{ads} will be blocked simultaneously. As a result, the competition yields an excessive coverage of adsorbed $(CH_3O)_{ads}$ and an insufficient coverage of OH_{ads} on the ligament surface. This imbalance adsorption between $(CH_3O)_{ads}$ and OH_{ads} should be responsible for the level-off of the peak current density in the electrolyte with high methanol concentrations (above 2 M, Fig. 6(a) and (b)). Additionally, the insufficient adsorption of OH_{ads} can induce the oxidation of Pd surface atoms at a more positive potential with increasing methanol concentration in the electrolyte. Thereby, the resultant delay formation of the Pd oxides on the ligament surface leads to the shift of the methanol oxidation peak towards positive directions (Fig. 6(a) and (c)).

Fig. 7(a) shows the effect of potential scan rate on the electro-oxidation of methanol on the npPd rods electrode with the 0.4 mg cm^{-2} loading in the 0.5 M methanol + 1.0 M KOH solution. It can be seen that the oxidation peak current density increases with the increasing of potential scan rate from 2 to 30 mV s^{-1}. Meanwhile, the methanol oxidation peak potentials slightly shift to positive directions along with the increase of scan rate. In addition, it can be revealed that there exists an approximate linear relationship between the oxidation peak current densities and the square root of scan rates ($v^{1/2}$), as shown in Fig. 7(b). Hence, we can rationally assume that the electrocatalytic oxidation towards methanol on the npPd rods electrode in alkaline solutions is controlled by the diffusion process [42,73], which is consistent with the typical three-dimensional bicontinuous interpenetrating ligament-channel structure of the npPd rods.

4. Conclusions

In summary, a peculiar npPd rods nanostructure with high specific surface area can be fabricated through the dealloying of the $Al_{80}Pd_{20}$ alloy in the dilute acidic solution (5 wt.% HCl). The as-fabricated npPd rods exhibit a typical three-dimensional bicontinuous interpenetrating ligament-channel structure and reveal a superior electrocatalytic performance toward methanol oxidation in the alkaline media. The electrocatalytic activity has a dependence on the metal loading on the GC electrode and it has been found that the npPd rods electrode with the 0.4 mg cm^{-2} loading possesses the best catalytic performance for methanol oxidation. When the methanol concentration exceeds 2 M in the KOH solution, there exists a level-off in the oxidation current density due to the competing adsorption mechanism of methoxyl ($(CH_3O)_{ads}$) and hydroxyl (OH_{ads}). The electro-oxidation of methanol on the npPd/C catalyst is a diffusion-controlled process. Significantly, differing from other Pd nanostructures, this npPd structure can have a mass production with a high purity level so as to meet the industrial requirement. Hence, these npPd rods will find their promising prospect in the field of direct methanol fuel cells, industrial catalysts, sensors, and so on.

Acknowledgments

The authors gratefully acknowledge financial support by the National Natural Science Foundation of China under grants 50971079 and 50831003, 2nd special support from China Postdoctoral Science Foundation (200902555), and 43rd China Postdoctoral Science Foundation.

References

[1] B.D. McNicol, D.A.J. Rand, K.R. Williams, J. Power Sources 83 (1999) 15–31.
[2] C. Rice, S. Ha, R.I. Masel, P. Waszczuk, A. Wieckowski, T. Barnard, J. Power Sources 111 (2002) 83–89.
[3] H.Q. Li, G.Q. Sun, Q. Jiang, M.Y. Zhu, S.G. Sun, Q. Xin, Electrochem. Commun. 9 (2007) 1410–1415.
[4] J. Erlebacher, M.J. Aziz, A. Karma, N. Dimitrov, K. Sieradzki, Nature 410 (2001) 450–453.
[5] Y. Ding, J. Erlebacher, J. Am. Chem. Soc. 125 (2003) 7772–7773.
[6] J.C. Thorp, K. Sieradzki, L. Tang, P.A. Crozier, A. Misra, M. Nastasi, D. Mitlin, S.T. Picraux, Appl. Phys. Lett. 88 (2006) 033110–33113.
[7] L. Sun, C.L. Chien, P.C. Searson, Chem. Mater. 16 (2004) 3125–3129.
[8] J.R. Hayes, A.M. Hodge, J. Biener, A.V. Hamza, K. Sieradzki, J. Mater. Res. 21 (2006) 2611–2616.
[9] D.V. Pugh, A. Dursun, S.G. Corcoran, J. Mater. Res. 18 (2003) 216–221.
[10] S. Kameoka, A.P. Tsai, Catal. Lett. 121 (2008) 337–341.
[11] Z.H. Zhang, Y. Wang, Z. Qi, W.H. Zhang, J.Y. Qin, J. Frenzel, J. Phys. Chem. C 113 (2009) 12629–12636.
[12] X.G. Wang, Z. Qi, C.C. Zhao, W.M. Wang, Z.H. Zhang, J. Phys. Chem. C 113 (2009) 13139–13150.
[13] H.B. Lu, Y. Li, F.H. Wang, Scr. Mater. 56 (2007) 165–168.
[14] Z. Qi, C.C. Zhao, X.G. Wang, J.K. Lin, W. Shao, Z.H. Zhang, X.F. Bian, J. Phys. Chem. C 113 (2009) 6694–6698.
[15] C.C. Zhao, Z. Qi, X.G. Wang, Z.H. Zhang, Corros. Sci. 51 (2009) 2120–2125.
[16] J.S. Yu, Y. Ding, C.X. Xu, A. Inoue, T. Sakurai, M.W. Chen, Chem. Mater. 20 (2008) 4548–4550.
[17] Y. Zhu, Y.Y. Kang, Z.Q. Zou, Q. Zhou, J.W. Zheng, B.J. Xia, H. Yang, Electrochem. Commun. 10 (2008) 802–805.
[18] F.L. Jia, K.W. Wong, R.X. Du, Electrochem. Commun. 11 (2009) 519–521.
[19] F.L. Jia, K.W. Wong, L.Z. Zhang, J. Phys. Chem. C 113 (2009) 7200–7206.
[20] C.W. Xu, H. Wang, P.K. Shen, S.P. Jiang, Adv. Mater. 19 (2007) 4256–4259.
[21] Z. Yin, H.J. Zheng, D. Ma, X.H. Bao, J. Phys. Chem. C 113 (2009) 1001–1005.
[22] C.X. Xu, L.Q. Wang, R.Y. Wang, K. Wang, Y. Zhang, F. Tian, Y. Ding, Adv. Mater. 21 (2009) 1–5.
[23] M. Grdeń, A. Piascik, Z. Koczorowski, A. Czerwiński, J. Electroanal. Chem. 532 (2002) 35–42.
[24] M. Baldauf, D.M. Kolb, Electrochim. Acta 38 (1993) 2145–2153.
[25] L.H. Dall'Antonia, G. Tremiliosi-Filho, G. Jerkiewicz, J. Electroanal. Chem. 502 (2001) 72–81.
[26] M. Grdeń, M. Łukaszewski, G. Jerkiewicz, A. Czerwiński, Electrochim. Acta 53 (2008) 7583–7598.
[27] J.T. Zhang, M.H. Huang, H.Y. Ma, F. Tian, W. Pan, S.H. Chen, Electrochem. Commun. 9 (2007) 1298–1304.
[28] W. Pan, X.K. Zhang, H.Y. Ma, J.T. Zhang, J. Phys. Chem. C 112 (2008) 2456–2461.
[29] P.N. Bartlett, B. Gollas, S. Guerin, J. Marwan, Phys. Chem. Chem. Phys. 4 (2002) 3835–3842.
[30] J.S. Gullón, A. Rodes, V. Moniel, A. Aldaz, J. Clavilier, J. Electroanal. Chem. 554–555 (2003) 273–284.
[31] X.B. Ge, X.L. Yan, R.Y. Wang, F. Tian, Y. Ding, J. Phys. Chem. C 113 (2009) 7379–7384.
[32] M.D. Obradovíc, A.V. Tripkovic, S.L. Gojkovic, Electrochim. Acta 55 (2009) 204–209.
[33] S.T. Nguyen, H.M. Law, H.T. Nguyen, N. Kristian, S.Y. Wang, Appl. Catal. B: Environ. 91 (2009) 507–515.
[34] X. Wang, Y.W. Tang, Y. Gao, T.H. Lu, J. Power Sources 175 (2008) 784–788.
[35] X.Z. Xue, J.J. Ge, C.P. Liu, W. Xing, T.H. Lu, Electrochem. Commun. 8 (2006) 1280–1286.
[36] T. Biegler, D.A.J. Rand, R. Woods, J. Electroanal. Chem. 29 (1971) 269–277.
[37] S.M. Choi, J.H. Kim, J.Y. Jung, E.Y. Yoon, W.B. Kim, Electrochim. Acta 53 (2008) 5804–5811.
[38] A. Czerwiński, R. Marassi, S. Zamponi, J. Electroanal. Chem. 316 (1991) 211–221.
[39] A. Rose, S. Maniguet, R.J. Mathew, C. Slater, J. Yao, A.E. Russell, Phys. Chem. Chem. Phys. 5 (2003) 3220–3225.
[40] Y.J. Huang, X.C. Zhou, J.H. Liao, C.P. Liu, T.H. Lu, W. Xing, Electrochem. Commun. 10 (2008) 621–624.
[41] H. Razmi, E. Habibi, H. Heidari, Electrochim. Acta 53 (2008) 8178–8185.
[42] W.Q. Zhou, C.Y. Zhai, Y.K. Du, J.K. Xu, P. Yang, Int. J. Hydrogen Energy 34 (2009) 9316–9323.
[43] Z.P. Sun, X.G. Zhang, Y.Y. Liang, H.L. Li, J. Power Sources 191 (2009) 366–370.
[44] C.W. Xu, Y.L. Liu, D.S. Yuan, Int. J. Electrochem. Sci. 2 (2007) 674–680.
[45] Y.W. Lee, S.B. Han, K.W. Park, Electrochem. Commun. 11 (2009) 1968–1971.
[46] M.S. Ureta-Zanartu, A. Alarcon, G. Munoz, C. Gutierrez, Electrochim. Acta 52 (2007) 7857–7864.
[47] X.W. Teng, X.Y. Liang, S. Maksimuk, H. Yang, Small 2 (2006) 249–253.
[48] R.N. Singh, A. Singh, Anindita, Int. J. Hydrogen Energy 34 (2009) 2052–2057.
[49] J.C. Huang, Z.L. Liu, C.B. He, L.M. Gan, J. Phys. Chem. C 109 (2005) 16644–16649.
[50] J. Yin, J.B. Jia, L.D. Zhu, Int. J. Hydrogen Energy 33 (2008) 7444–7447.
[51] Y.Y. Mu, H.P. Liang, J. Hu, J.S. Hu, L. Jiang, L.J. Wan, J. Phys. Chem. B 9 (2005) 22212–22216.
[52] Z.L. Liu, X.H. Zhang, L. Hong, Electrochem. Commun. 11 (2009) 925–928.
[53] R. Manohara, J.B. Goodenough, J. Mater. Chem. 2 (1992) 875–887.
[54] Y.X. Chen, A. Miki, S. Ye, H. Sakai, M. Osawa, J. Am. Chem. Soc. 125 (2003) 3680–3681.
[55] W.F. Lin, J.T. Wang, R.F. Savinell, J. Electrochem. Soc. 144 (1997) 1917–1922.
[56] Y.J. Gu, W.T. Wang, Langmuir 22 (2006) 11447–11452.
[57] C.H. Yen, K. Shimizu, Y.Y. Lin, F. Bailey, I.F. Cheng, C.M. Wai, Energy Fuels 21 (2007) 2268–2271.
[58] L.F. Liu, E. Pippel, R. Scholz, U. Gösele, Nano Lett. 9 (2009) 4352–4358.
[59] T.C. Deivaraj, J.Y. Lee, J. Power Sources 142 (2005) 43–49.
[60] O.T.M. Musthafa, S. Sampath, Chem. Commun. (2008) 67–69.
[61] T. Maiyalagan, J. Solid State Electrochem. 13 (2009) 1561–1566.
[62] Y.W. Qu, X.L. Cui, X.Y. Zhang, Z.Y. Jiang, J. Power Sources 195 (2010) 1365–1369.
[63] M.C. Morin, C. Lamy, J.M. Léger, J. Electroanal. Chem. 283 (1990) 287–302.
[64] J.Q. Ye, J.P. Liu, C.W. Xu, S.P. Jiang, Y.X. Tong, Electrochem. Commun. 9 (2007) 2760–2763.
[65] Q.G. He, W. Chen, S. Mukerjee, S.W. Chen, F. Laufek, J. Power Sources 187 (2009) 298–304.
[66] M. Sevilla, C. Sanchís, T. Valdés-Solís, E. Morallón, A.B. Fuertes, Electrochim. Acta 54 (2009) 2234–2238.
[67] Z.X. Liang, T.S. Zhao, J.B. Xu, L.D. Zhu, Electrochim. Acta 54 (2009) 2203–2208.
[68] T. Yajima, H. Uchida, M. Watanabe, J. Phys. Chem. B 108 (2004) 2654–2659.
[69] T. Yajima, N. Wakabayashi, H. Uchida, M. Watanabe, Chem. Commun. (2003) 828–829.
[70] R.J. Levis, Z.C. Jiang, N. Winograd, J. Am. Chem. Soc. 111 (1989) 4605–4612.
[71] C.J. Zhang, P. Hu, J. Chem. Phys. 115 (2001) 7182–7186.
[72] T. Takamura, K. Minamiyama, J. Electrochem. Soc. 112 (1965) 333–335.
[73] A.J. Bard, L. Faulkner, Electrochemical Methods: Fundamentals and Applications, Wiley, New York, 1980.